



Cite this: *J. Mater. Chem. B*, 2017, 5, 5648

## Toxicity and oxidative stress responses induced by nano- and micro-CoCrMo particles†‡

Andrea L. Armstead,<sup>ab</sup> Thiago A. Simoes,<sup>c</sup> Xianfeng Wang,<sup>ad</sup> Rik Brydson,<sup>c</sup> Andy Brown,<sup>c</sup> Bing-Hua Jiang,<sup>e</sup> Yon Rojanasakul<sup>bf</sup> and Bingyun Li<sup>id</sup> §\*<sup>abf</sup>

Metal implants are used routinely during total hip and knee replacements and are typically composed of cobalt chromium molybdenum (CoCrMo) alloys. CoCrMo “wear particles”, in the nano- and micro-size ranges, are generated *in situ*. Meanwhile, occupational exposure to CoCrMo particles may be associated with the development of industrial dental worker’s pneumoconiosis. In this study, we report that both nano- and micro-CoCrMo induced a time and dose-dependent toxicity in various cell types (*i.e.* lung epithelial cells, osteoblasts, and macrophages), and the effects of particle size on cell viability and oxidative responses were interesting and cell specific. Our findings highlight the potential roles that nano- and micro-CoCrMo, whether exposure is due to inhalation or implant wear, and the associated oxidative stress may play in the increasingly reported implant loosening, osteolysis, and systemic complications in orthopaedic patients, and may explain the risk of lung diseases in dental workers.

Received 18th May 2017,  
Accepted 13th June 2017

DOI: 10.1039/c7tb01372h

rsc.li/materials-b

### 1. Introduction

Over a million total hip replacement procedures are performed each year and cobalt chromium molybdenum (CoCrMo) alloys have been widely used as metal-on-metal or metal-on-polyethylene implant devices. While metal implant devices offer advantages, such as high strength, evidence has emerged that metal (*e.g.* CoCrMo) implant devices may generate wear particles *in situ*, within the micro- and nano-size range, as a result of implant breakdown between the articulating joint surfaces.<sup>1,2</sup> The generation of wear particles increases when the implant is improperly aligned, causing aseptic loosening of the joint and uneven wear and damage within the implant area.<sup>2,3</sup> The specific role of CoCrMo particles in joint loosening or associated osteolysis

remains unclear, although several sources suggest that the presence of wear particles within the joint cavity promotes a localized inflammatory response succeeded by resorptive bone loss.<sup>4–7</sup> Given this evidence and emerging concerns regarding the long term effects of CoCrMo particle exposure in joint replacement patients, the toxicity of CoCrMo wear particles has recently gained great interest both *in vitro*<sup>8–12</sup> and *in vivo*.<sup>13–15</sup>

In addition to “internal” and localized CoCrMo particle exposure due to implant wear, alternative routes of exposure such as inhalation or secondary exposure(s) due to particle translocation or migration from the initial site must be considered. For instance, CoCrMo particle inhalation may occur during manufacturing and production in the medical device industry, thereby presenting an occupational exposure hazard. Although occupational exposure to CoCrMo particles has not been directly reported to date in orthopaedic implant manufacturing settings, pulmonary exposure to CoCrMo “dusts” with a similar composition to metal orthopaedic implant material have been reported previously in dental implant manufacturing settings.<sup>16</sup> Inhalation of CoCrMo particles might have been associated with the “dental technician’s pneumoconiosis” (DTP) in a number of cases.<sup>17</sup> In other industrial and manufacturing settings, inhalation of cobalt-containing metal “dusts”, such as tungsten carbide cobalt (WC-Co), has been well-associated with the development of pneumoconiosis, occupational asthma and lung disease with an increased risk of lung cancer.<sup>18,19</sup> For DTP resulting from exposure to CoCrMo particles, patients develop lung disease with a similar clinical presentation to hard metal lung disease (HMLD) resulting from occupational inhalation of WC-Co particles,<sup>3,17,20</sup> therefore, we believe it is pertinent to examine the effects of CoCrMo particle exposure in a relevant *in vitro* pulmonary model.

<sup>a</sup> Department of Orthopaedics, School of Medicine, West Virginia University, Morgantown, WV 26506, USA. E-mail: bili@hsc.wvu.edu;  
Web: <http://medicine.hsc.wvu.edu/ortho-bli/>; Fax: +1-304-293-7070;  
Tel: +1-304-293-1075

<sup>b</sup> School of Pharmacy, West Virginia University, Morgantown, WV 26506, USA

<sup>c</sup> Institute for Materials Research, School of Chemical and Process Engineering, University of Leeds, LS2 9JT, UK

<sup>d</sup> Key Laboratory of Textile Science & Technology, Ministry of Education, College of Textiles, Donghua University, Shanghai 201620, China

<sup>e</sup> Department of Pathology, Anatomy and Cell Biology, Thomas Jefferson University, Philadelphia, PA 19107, USA

<sup>f</sup> Mary Babb Randolph Cancer Center, Morgantown, WV 26506, USA

† The abstract was presented at the Orthopaedic Research Society Annual Meeting, March 2016.

‡ Electronic supplementary information (ESI) available. See DOI: 10.1039/c7tb01372h

§ Present address: Biomaterials, Bioengineering & Nanotechnology Laboratory, Department of Orthopaedics, School of Medicine, West Virginia University, 1 Medical Center Drive, Morgantown, WV 26506-9196, USA.

There is also emerging evidence that particles within the nano-size range are capable of tissue translocation and migration to other organs, such as the liver, spleen or lungs,<sup>21–23</sup> where tissue deposition occurs and a secondary particle exposure is generated. This phenomenon may occur for CoCrMo particles generated internally at orthopaedic implant sites and the potential for secondary CoCrMo particle toxicity at sites distant from the initial exposure cannot be excluded. Therefore, it is critically important to understand the full range of effects of CoCrMo particle exposure on a variety of cell types which are potential targets for CoCrMo particle exposure, whether the initial exposure was due to internal particle generation from orthopaedic implants or from external sources such as inhalation in occupational settings. The goal of the current study was to examine the toxicity and oxidative stress response induced by nano- and micro-sized CoCrMo particles in various cell types using a nanotoxicity model recently developed in our lab.<sup>24</sup> We hypothesized that nano- and micro-CoCrMo would exert cell-specific, time and dose-dependent toxicity and oxidative stress response in lung epithelial cells, osteoblasts, and macrophages.

## 2. Methods

### 2.1. Materials and reagents

CoCrMo microparticles (micro-CoCrMo) in the form of gas atomized powders from ASTM75 implants were used as received from Sandvik Osprey (Sandviken, Sweden); the chemical composition was  $63.3 \pm 1.1$  wt% Co,  $30.2 \pm 0.7$  wt% Cr and  $6.5 \pm 1.2$  wt% Mo. Human lung bronchial epithelial BEAS-2B cells,<sup>24</sup> THP-1 (TIB-202) human monocytes/macrophages<sup>25</sup> and h.FOB1.19 (CRL-11372) human osteoblast cells<sup>26–29</sup> from our previous studies were from American Type Tissue Collection (ATCC; Manassas, VA). Dulbecco's Modified Eagle's Medium (DMEM), Ham's F12 Medium, sterile phosphate buffered saline (PBS), 0.25% trypsin/ethylenediaminetetraacetic acid (EDTA), fetal bovine serum (FBS), the G418 sulfate (geneticin) cell selection agent and penicillin/streptomycin were purchased from Lonza (Allendale, NJ). RPMI-1640 culture medium was purchased from ATCC. Isopropanol, hydrochloric acid, Triton-X-100, thiazolyl blue tetrazolium bromide (MTT reagent), 2',7'-dichlorofluorescein diacetate (DCF), dihydroethidium (DHE) and phorbol-12-myristate-13-acetate (PMA) were purchased from Sigma-Aldrich (St. Louis, MO).

### 2.2. Particle preparation and characterization

CoCrMo nanoparticles (nano-CoCrMo) were obtained *via* mechanical milling of micro-CoCrMo (see the ESI†). Dilute particle suspensions, ranging from 0.1 to 1000  $\mu\text{g mL}^{-1}$ , were prepared in DMEM containing 10% FBS and used immediately on the day of each experiment. The particle size of nano-CoCrMo was analyzed using transmission electron microscopy (TEM). Average particle size was achieved by measuring the Feret diameter of *ca.* 300 particles, which is defined as the distance between the most widely spaced nanoparticles in an agglomerate.<sup>30</sup> The particle size of micro-CoCrMo was characterized using scanning electron microscopy (SEM). In addition,

the average sizes of nano- and micro-CoCrMo in suspension in 10% FBS were determined using dynamic light scattering (DLS, Malvern Zetasizer version 7.01, Malvern Instruments). The CoCrMo particles had a zeta potential of  $-25$  mV and showed negligible aggregations in suspension at short time periods (*e.g.* 24 h).<sup>31</sup>

### 2.3. Cell culture and THP-1 macrophage differentiation

THP-1 monocytes were maintained in the suspension culture and upon confluency, THP-1 cells were transferred and centrifuged to form pellets. The cell pellet was re-suspended in RPMI containing PMA which induces THP-1 monocytes to undergo macrophage (M0) differentiation, and plated in a 96-well culture plate. More details of the cell culture of BEAS-2B, osteoblasts (OBs), and macrophages (M0) are provided in the ESI.†

### 2.4. CoCrMo particle assay interference

Prior to execution of the cell viability and oxidative stress assays, the potential interference of CoCrMo particles was examined under the experimental conditions (see the ESI.†).

### 2.5. CoCrMo particle exposure

Exposure to nano- and micro-CoCrMo was achieved by aspirating the media from each well and immediately replacing it with an equivalent volume of CoCrMo particle suspension at a concentration of 0.1–1000  $\mu\text{g mL}^{-1}$ . Cell plates were then incubated at 37 °C and 5% CO<sub>2</sub> for exposure periods of 6, 12, 24 and 48 h.

### 2.6. Cell viability assay

For the viability assay, cells were exposed to either nano- or micro-CoCrMo at concentrations of 0.1, 1, 10, 100 and 1000  $\mu\text{g mL}^{-1}$  for exposure periods of 6, 12, 24 and 48 h. Following particle treatment, cells were rinsed once with sterile PBS to remove traces of media and excess particles. Then, 100  $\mu\text{L}$  of unsupplemented DMEM was added to each well, followed by the addition of 10  $\mu\text{L}$  of MTT reagent to achieve a final concentration of 0.5  $\text{mg mL}^{-1}$  MTT reagent per well. Cells were incubated for 2 h at 37 °C and 5% CO<sub>2</sub> to allow the conversion of the soluble salt (yellow) to formazan crystals (purple). Crystal formation was confirmed using light microscopy. 100  $\mu\text{L}$  of solubilization solution (0.1 M HCl in isopropanol with 10% Triton-X) was then added to each well to dissolve the formazan crystals and the absorbance of each well was recorded at 570 nm using a Bio-Tek  $\mu\text{Quant}$  microplate reader (Winooski, VT). Blank values were subtracted from absorbance readings. Cell viability was calculated by dividing the absorbance of particle treated cells by the absorbance of control cells receiving media treatment only and converted to percentage; control cells represented 100% viability.

### 2.7. Oxidative stress assay

Oxidative stress was examined at the same CoCrMo particle concentrations and exposure ranges described for the viability assay (above). Following particle treatment, cells were rinsed once with sterile PBS to remove traces of media and excess particles. Oxidative stress was then determined by the addition of 10  $\mu\text{M}$  DCF or DHE in PBS following particle treatment.

Plates were incubated for 15 min in the dark and then fluorescence intensity of each well was quantified at 520 nm for DCF or 620 nm for DHE using a Bio-Tek Synergy H4 plate reader (Winooski, VT). The relative fluorescence of particle-treated cells was calculated as fold over control.

### 2.8. Statistical analyses

All experiments were performed in triplicate and data are presented as mean  $\pm$  standard deviation. Statistical analysis was carried out by two-way analysis of variance (ANOVA) using GraphPad Prism 6 software (La Jolla, CA). *P* values  $< 0.05$  were considered significant.

## 3. Results

### 3.1. CoCrMo particle characterization and assay interference

TEM and SEM examination showed that the nano- and micro-CoCrMo had average sizes of  $35.4 \pm 30.4$  nm (Fig. 1A and C) and  $4.8 \pm 3.0$   $\mu\text{m}$  (Fig. 1B and D), respectively. DLS analysis indicated that nano-CoCrMo averaged 54 nm and micro-CoCrMo averaged 5.0  $\mu\text{m}$  in suspensions. EDX confirmed that the composition of nano- and micro-CoCrMo were largely Co, Cr and Mo (Fig. S1, ESI $\ddagger$ ). We did not find any significant CoCrMo particle interference in our assays; no significant auto-reduction of the MTT dye was identified in the viability assay

(Fig. S2, ESI $\ddagger$ ) and no significant changes in DCF/DHE fluorescence were observed due to CoCrMo particles under the assay conditions tested (Fig. S3, ESI $\ddagger$ ).

### 3.2. CoCrMo effects on cell viability

BEAS-2B, OBs and macrophages were exposed to nano- and micro-CoCrMo at concentrations of 0.1, 1, 10, 100 and 1000  $\mu\text{g mL}^{-1}$  for durations of 6, 12, 24 and 48 h. For BEAS-2B, the average cell viability was about 90–98% (vs. control of 100%) for cells exposed to nano- and micro-CoCrMo at concentrations of 0.1, 1 and 10  $\mu\text{g mL}^{-1}$  for durations of 6–48 h; the cell viability tended to decrease with increasing particle exposure time from 6 h to 48 h at concentrations of 100 and 1000  $\mu\text{g mL}^{-1}$  (Fig. 2). In cells exposed to nano-CoCrMo (Fig. 2A), a significant reduction in viability (compared to control) was observed at 100  $\mu\text{g mL}^{-1}$  after 12, 24 and 48 h of exposure and at the highest concentration of 1000  $\mu\text{g mL}^{-1}$  after 6–48 h of exposure. Similarly, in BEAS-2B cells exposed to micro-CoCrMo (Fig. 2B), a significant reduction in viability (compared to control) was observed at 100  $\mu\text{g mL}^{-1}$  after 12, 24 and 48 h of exposure and at the highest concentration of 1000  $\mu\text{g mL}^{-1}$  after 6–48 h of exposure. When comparing the toxicity of nano- and micro-CoCrMo under identical conditions, nano-CoCrMo caused significantly less toxicity than micro-CoCrMo in BEAS-2B cells at 100  $\mu\text{g mL}^{-1}$  after 24 and 48 h of exposure and at 1000  $\mu\text{g mL}^{-1}$  after 6 and

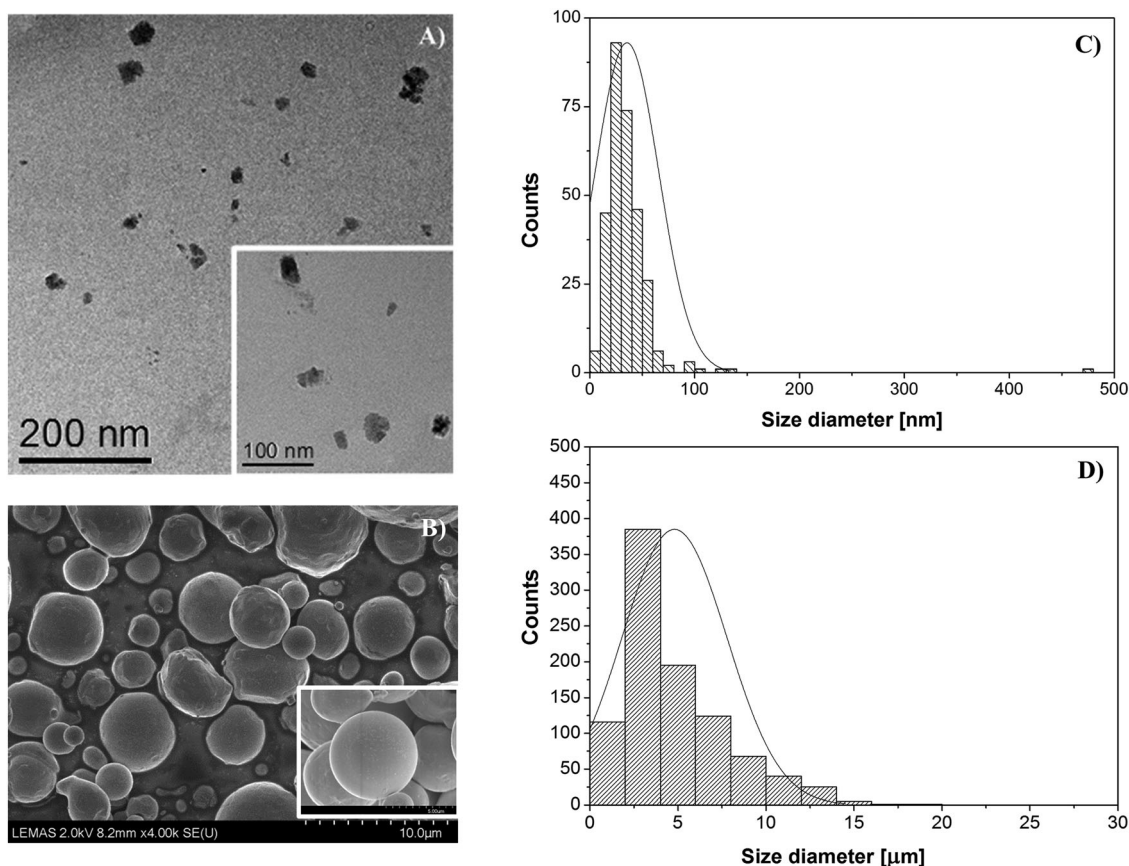


Fig. 1 (A and B) Images and (C and D) particle size distribution of (A and C) nano- and (B and D) micro-CoCrMo.

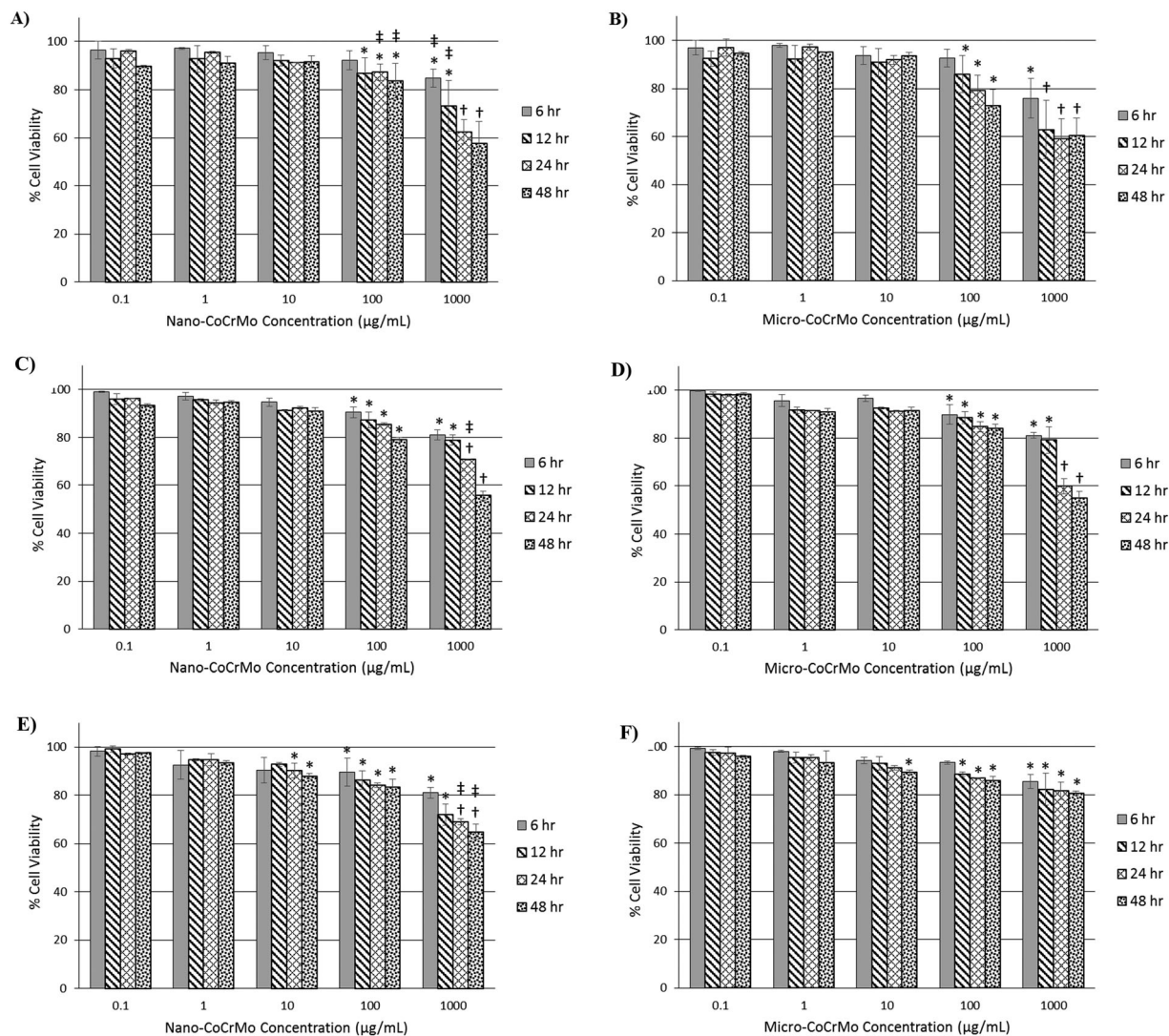


Fig. 2 Viability of (A and B) BEAS-2B lung epithelial cells, (C and D) osteoblasts, and (E and F) macrophages after exposure to (A, C and E) nano- and (B, D and F) micro-CoCrMo (\* $P < 0.05$ , † $P < 0.01$  compared to control; ‡ $P < 0.05$  vs. micro-CoCrMo).

12 h of exposure; toxicity was similar for  $1000 \mu\text{g mL}^{-1}$  nano- and micro-CoCrMo after 24 and 48 h of exposure.

For osteoblasts (OBs), cell viability remained high ( $>90\%$ ) over the exposure periods tested (6–48 h) for  $0.1$ – $10 \mu\text{g mL}^{-1}$  nano- and micro-CoCrMo (Fig. 2C). At  $100$  and  $1000 \mu\text{g mL}^{-1}$ , a significant decrease in cell viability (compared to control) was observed after 6–48 h of exposure of nano- (Fig. 2C) and micro-CoCrMo (Fig. 2D) and the cell viability decreased with increasing exposure time. There were no significant differences in the toxicity of nano- and micro-CoCrMo over the concentration and exposure ranges studied, with the exception of  $1000 \mu\text{g mL}^{-1}$ , where nano-CoCrMo caused significantly less toxicity than micro-CoCrMo in OBs after 24 h of exposure ( $\sim 70\%$  vs.  $\sim 60\%$  remaining cell viability, respectively).

In macrophages (M0), cell viability remained  $>90\%$  for the lowest concentrations of  $0.1$  and  $1 \mu\text{g mL}^{-1}$  over the 6–48 h exposure period for both nano- and micro-CoCrMo (Fig. 2). M0 exposed to nano-CoCrMo had significantly reduced viability

(compared to control) after 24 and 48 h of exposure to  $10 \mu\text{g mL}^{-1}$  (Fig. 2E); no significant toxicity was observed between CoCrMo particles and controls at this concentration in either BEAS-2B or OBs under these conditions. Significantly reduced cell viability was also observed for the micro-CoCrMo at  $10 \mu\text{g mL}^{-1}$  after 48 h of exposure (Fig. 2F). Moreover, at  $100$  and  $1000 \mu\text{g mL}^{-1}$ , a significant decrease in cell viability (compared to control) was observed for both nano- and micro-CoCrMo at the exposure times studied except at 6 h of exposure to  $100 \mu\text{g mL}^{-1}$  micro-CoCrMo. When compared directly, M0 viability after exposure to  $1000 \mu\text{g mL}^{-1}$  nano-CoCrMo for 24 and 48 h was significantly lower than M0 exposed to micro-CoCrMo under identical conditions.

### 3.3. CoCrMo effects on oxidative stress

Oxidative stress was measured in the form of DCF/DHE fluorescence after exposure to nano- and micro-CoCrMo under identical exposure conditions tested in the viability assay. Compared to control, there was a significant increase in DCF fluorescence in

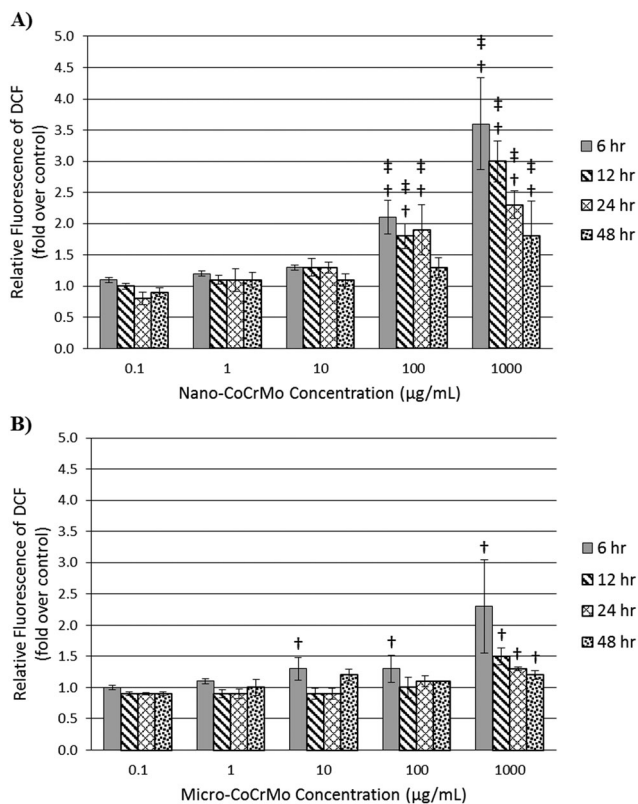


Fig. 3 BEAS-2B oxidative stress measured *via* fluorescence intensity of DCF after exposure to (A) nano- and (B) micro-CoCrMo (\* $P < 0.05$ , † $P < 0.01$  compared to control; ‡ $P < 0.05$  vs. micro-CoCrMo).

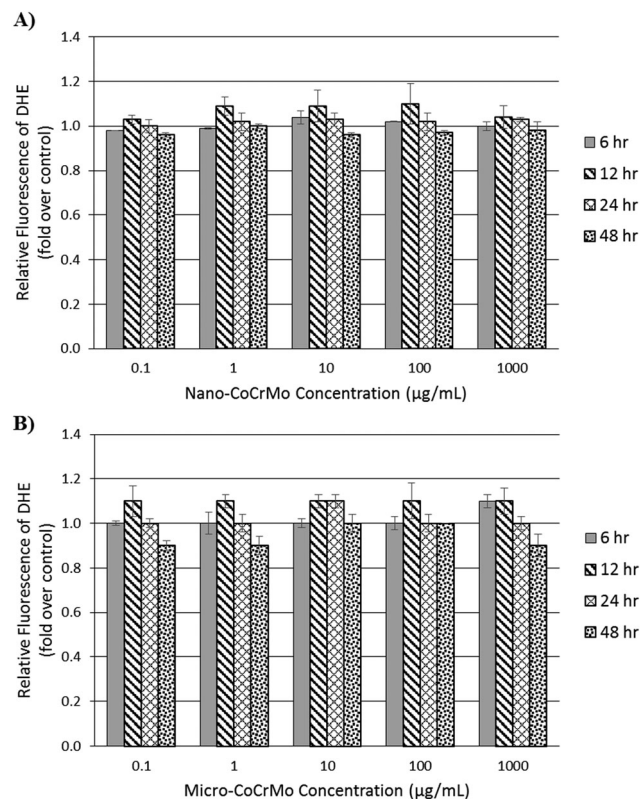


Fig. 4 BEAS-2B oxidative stress measured *via* fluorescence intensity of DHE after exposure to (A) nano- and (B) micro-CoCrMo (\* $P < 0.05$ , † $P < 0.01$  compared to control; ‡ $P < 0.05$  vs. micro-CoCrMo).

BEAS-2B cells exposed to  $100 \mu\text{g mL}^{-1}$  nano-CoCrMo after 6, 12 and 24 h of exposure and at  $1000 \mu\text{g mL}^{-1}$  after 6, 12, 24 and 48 h of exposure; a maximum of 3.5 fold increase in DCF fluorescence was observed in BEAS-2B cells exposed to  $1000 \mu\text{g mL}^{-1}$  nano-CoCrMo after 6 h of exposure, after which DCF fluorescence decreased with increasing exposure time (Fig. 3A). In BEAS-2B cells exposed to micro-CoCrMo, a significant increase in DCF fluorescence was observed after 6 h of exposure to 10 and  $100 \mu\text{g mL}^{-1}$  and after 6, 12, 24 and 48 h of exposure to  $1000 \mu\text{g mL}^{-1}$  micro-CoCrMo; a maximum of 2.3 fold increase in DCF fluorescence was observed in cells exposed to  $1000 \mu\text{g mL}^{-1}$  micro-CoCrMo after 6 h of exposure (Fig. 3B). At  $1000 \mu\text{g mL}^{-1}$  of both nano- and micro-CoCrMo, the DCF fluorescence decreased with increasing exposure time (Fig. 3). In addition, nano-CoCrMo caused a significantly greater change in DCF fluorescence compared to micro-CoCrMo after 6, 12 and 24 h of exposure to  $100 \mu\text{g mL}^{-1}$  and after 6, 12, 24 and 48 h of exposure to  $1000 \mu\text{g mL}^{-1}$  (Fig. 3).

For dihydroethidium (DHE), no significant differences, compared to control, were observed in BEAS-2B fluorescence after exposure to nano-CoCrMo (Fig. 4A) or micro-CoCrMo (Fig. 4B). The observed DHE fluorescence in BEAS-2B cells exposed to both nano- and micro-CoCrMo was about the same as the control cells at all concentrations ( $0.1$ – $1000 \mu\text{g mL}^{-1}$ ) and exposure times (6–48 h) studied.

In osteoblasts (OBs), nano-CoCrMo caused a significant increase in 2',7'-dichlorofluorescein diacetate (DCF) fluorescence, compared to control, at  $0.1 \mu\text{g mL}^{-1}$  after 12 h, at  $100 \mu\text{g mL}^{-1}$

after 12 and 24 h and a maximum increase in DCF fluorescence at  $1000 \mu\text{g mL}^{-1}$  after 24 h of exposure, about 1.5-fold higher than control (Fig. 5A). Exposure to micro-CoCrMo caused significantly increased DCF fluorescence, compared to control, after 12 h of exposure to 0.1, 10, 100 and  $1000 \mu\text{g mL}^{-1}$  and after 24 h of exposure to  $1000 \mu\text{g mL}^{-1}$  (Fig. 5B). Overall, nano-CoCrMo caused significantly higher DCF fluorescence than micro-CoCrMo in OBs after 24 h of exposure to 100 and  $1000 \mu\text{g mL}^{-1}$  (Fig. 5).

A varying effect on dihydroethidium (DHE) fluorescence was observed in osteoblasts (OBs) exposed to nano- and micro-CoCrMo (Fig. 6). Compared to control, a significant increase in DHE fluorescence was observed in OBs exposed to nano-CoCrMo at  $0.1 \mu\text{g mL}^{-1}$  after 48 h, at  $1 \mu\text{g mL}^{-1}$  after 6, 24 and 48 h, at  $10 \mu\text{g mL}^{-1}$  after 12, 24 and 48 h, at  $100 \mu\text{g mL}^{-1}$  after 6 and 12 h and at  $1000 \mu\text{g mL}^{-1}$  after 6, 12, 24, and 48 h of exposure (Fig. 6A). For micro-CoCrMo, a significant increase in DHE, compared to control, was observed for  $0.1$ – $1000 \mu\text{g mL}^{-1}$  after 6 h of exposure and for 1, 10, 100 and  $1000 \mu\text{g mL}^{-1}$  after 12 h of exposure (Fig. 6B). Compared to micro-CoCrMo, nano-CoCrMo caused significantly less DHE fluorescence at 0.1 and  $1 \mu\text{g mL}^{-1}$  after 6 h and at 1, 10 and  $100 \mu\text{g mL}^{-1}$  after 12 h; however, at  $1000 \mu\text{g mL}^{-1}$ , nano-CoCrMo caused significantly higher DHE fluorescence than micro-CoCrMo after 6, 24 and 48 h of exposure (Fig. 6A).

In macrophages (M0), nano- and micro-CoCrMo caused a significant increase in 2',7'-dichlorofluorescein diacetate (DCF) fluorescence, compared to control, at all concentrations

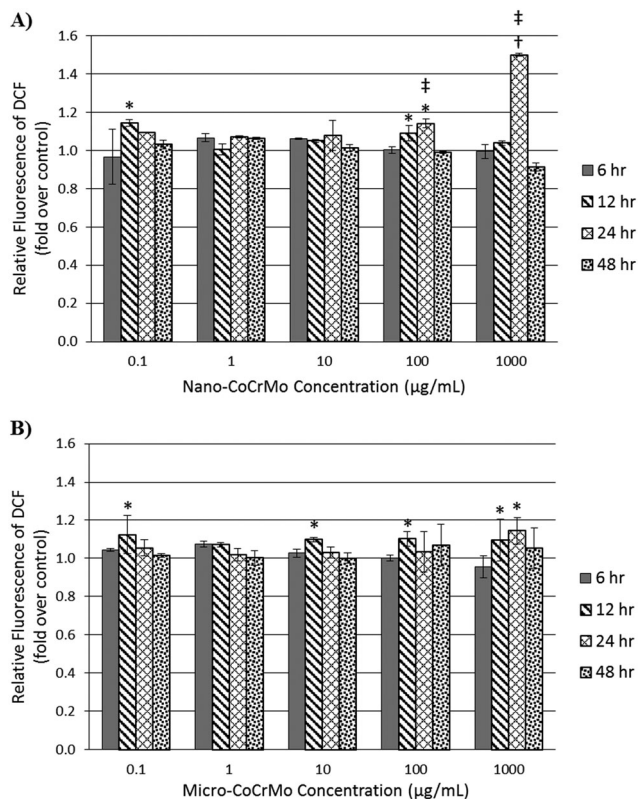


Fig. 5 Osteoblast oxidative stress measured via fluorescence intensity of DCF after exposure to (A) nano- and (B) micro-CoCrMo (\* $P < 0.05$ , † $P < 0.01$  compared to control; ‡ $P < 0.05$  vs. micro-CoCrMo).

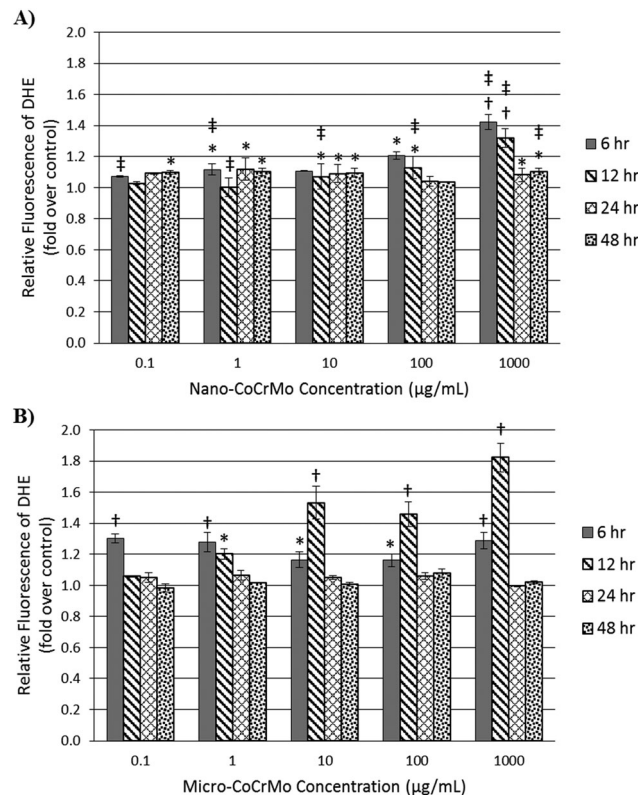


Fig. 6 Osteoblast oxidative stress measured via fluorescence intensity of DHE after exposure to (A) nano- and (B) micro-CoCrMo (\* $P < 0.05$ , † $P < 0.01$  compared to control; ‡ $P < 0.05$  vs. micro-CoCrMo).

(0.1–1000  $\mu\text{g mL}^{-1}$ ) and exposure times tested (Fig. 7). The maximum increase in DCF was observed at 1000  $\mu\text{g mL}^{-1}$  after 6 and 12 h of exposure (Fig. 7) for both nano- and micro-CoCrMo. Comparing directly, nano-CoCrMo caused significantly less DCF fluorescence than micro-CoCrMo after 12 h of exposure to 0.1, 10 and 100  $\mu\text{g mL}^{-1}$ ; however, nano-CoCrMo caused significantly higher DCF fluorescence than micro-CoCrMo after 6 and 12 h of exposure to 100  $\mu\text{g mL}^{-1}$  and after 24 and 48 h of exposure to 1000  $\mu\text{g mL}^{-1}$  (Fig. 7).

Significantly increased dihydroethidium (DHE) fluorescence, compared to control, was observed in macrophages (M0) exposed to nano-CoCrMo at all concentrations tested (0.1–1000  $\mu\text{g mL}^{-1}$ ) after 6, 12 and 24 h of exposure; no changes in DHE were observed after 48 h of exposure at any concentration (Fig. 8A). In M0 exposed to micro-CoCrMo, a significant increase in DHE fluorescence was observed after 6 and 12 h of exposure to 0.1–1000  $\mu\text{g mL}^{-1}$ ; DHE levels were similar to control at all concentrations after 24 and 48 h of exposure to micro-CoCrMo (Fig. 8B). Compared to micro-CoCrMo, nano-CoCrMo caused significantly higher DHE levels in M0 at all concentrations (0.1–1000  $\mu\text{g mL}^{-1}$ ) after 12 and 24 h of exposure (Fig. 8).

## 4. Discussion

Nanoparticles, due to their smaller size, have a higher capacity (compared to microparticles) to enter the circulatory system

and deposit in tissues and organs such as the liver, spleen, kidneys, lymph nodes and lungs,<sup>3,32–34</sup> and the potential systemic effects of nanoparticle exposure could be of importance.<sup>35</sup> However, the role of nanoparticles and microparticles for orthopaedic implant wear in systemic responses is unknown although patients who undergo CoCrMo joint replacements have presented translocation and deposition of CoCrMo wear particles in lymph nodes, liver and spleen.<sup>3,36</sup> Meanwhile, inhalation of cobalt-containing metal particles may be associated with dental technician's pneumoconiosis,<sup>16,17,20,37</sup> and CoCrMo wear particles have also been a major concern of local toxicity and inflammation. Therefore, the goal of this study was to examine the toxic effects of nano- and micro-sized CoCrMo particles, originating from ASTM F75 orthopaedic implant materials, in a range of relevant cell types representing the potential routes of exposures, including lung epithelial cells, osteoblasts, and macrophages.

Our studies suggest that both nano- and micro-CoCrMo can induce toxicity in all cell types studied and the responses of cell viability and oxidative stress are specific to dose, exposure time and cell type. Across the three cell types tested, at low concentrations (*i.e.* 0.1 and 1  $\mu\text{g mL}^{-1}$ ), nano- and micro-CoCrMo did not cause significant toxicity in our viability assay. Typically, in the presence of small amounts of foreign particles, cells may isolate the particles in internal phagolysosomal compartments, which could prohibit them from further interacting with other

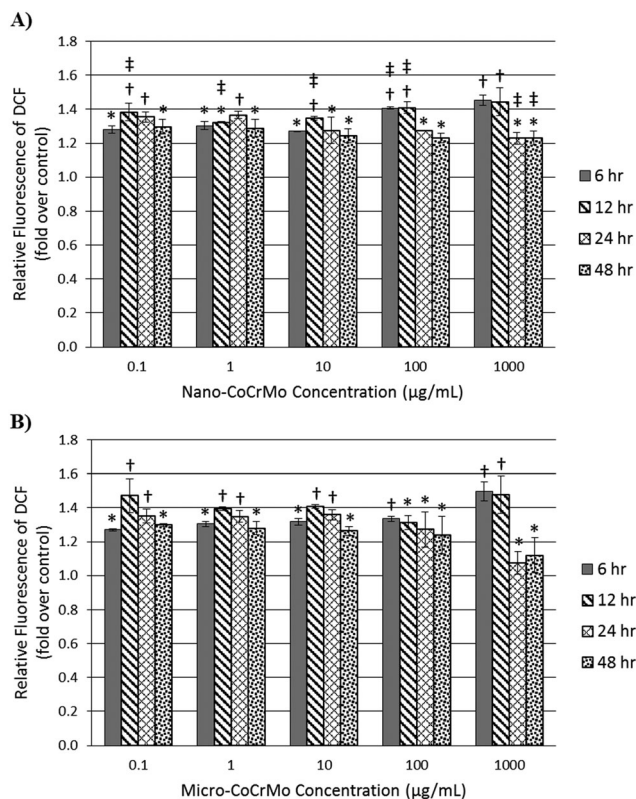


Fig. 7 Macrophage oxidative stress measured *via* fluorescence intensity of DCF after exposure to (A) nano- and (B) micro-CoCrMo (\* $P < 0.05$ , † $P < 0.01$  compared to control; ‡ $P < 0.05$  vs. micro-CoCrMo).

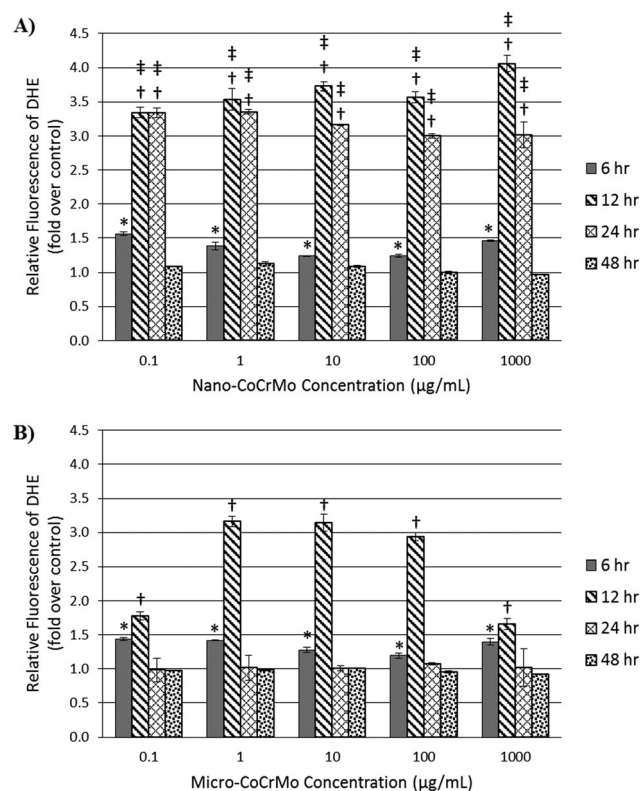


Fig. 8 Macrophage oxidative stress measured *via* fluorescence intensity of DHE after exposure to (A) nano- and (B) micro-CoCrMo (\* $P < 0.05$ , † $P < 0.01$  compared to control; ‡ $P < 0.05$  vs. micro-CoCrMo).

cellular components thereby preventing extensive cellular toxicity.<sup>11,38</sup> The similarity in low toxicity between the nano- and micro-CoCrMo reported here in lung epithelial cells, osteoblasts and macrophages at concentrations less than  $10 \mu\text{g mL}^{-1}$  seems to support the high biocompatibility of CoCrMo alloys in orthopaedic settings;<sup>39</sup> CoCrMo has been used prevalently in orthopaedic surgeries.<sup>3</sup> At high concentrations (*i.e.* 100 and  $1000 \mu\text{g mL}^{-1}$  for BEAS-2B and OB cells, and 10, 100 and  $1000 \mu\text{g mL}^{-1}$  for M0 cells), both nano- and micro-CoCrMo could lead to a significant decrease in viability in all cell types tested. It was reported that significant toxicity was observed in osteoblast-like cells exposed to  $\geq 100 \mu\text{g mL}^{-1}$  micro-CoCr alloy particles after 24 and 48 h of exposure.<sup>40</sup> The current study provides direct evidence that nano- and micro-CoCrMo cause toxicity toward lung epithelial cells *in vitro*; although lung epithelial cells are not a direct site of exposure in the case of orthopaedic joint wear, we speculate that these data may help in explaining the risk of lung disease in dental workers<sup>16,17,20,37,41,42</sup> and highlighting the need for further examination of pulmonary toxicity caused by CoCrMo particles, whether exposure is due to inhalation (in the case of DTP) or tissue migration of implant wear particles to the lungs.

One would normally expect that nanoparticles exert greater toxic effects than microparticles of the same chemical composition due to their smaller size and increased surface area.<sup>31,33,43–45</sup> However, in this study, no significant differences

in cell viability were observed between nano- and micro-CoCrMo exposures in most of the concentrations and exposure times studied. Interestingly, compared to micro-CoCrMo, nano-CoCrMo led to significantly lower viability of macrophages and significantly higher viability of lung epithelial cells and osteoblasts at  $1000 \mu\text{g mL}^{-1}$ . In macrophages, it was believed that nanoparticles, due to their smaller size and thereby faster degradation at a given pH, could lead to more impairment in phagocytosis and be more toxic to macrophages compared to microparticles.<sup>46–48</sup> In this case, it is possible that differences in the uptake of nano- and micro-CoCrMo could have contributed to the higher toxicity of nano-CoCrMo, as smaller particles may be more frequently and rapidly phagocytosed compared to the larger micro-CoCrMo. It is not clear why nano-CoCrMo was less toxic, compared to micro-CoCrMo, to lung epithelial cells and osteoblasts in this study and further investigations are much needed.

Oxidative stress has been implicated in age-related bone resorption and osteoporosis<sup>49</sup> and in the toxicity of CoCrMo particles in fibroblasts,<sup>50–52</sup> and may also play a role in the progression of lung diseases,<sup>53</sup> such as those caused by cobalt-containing metal exposures.<sup>54</sup> Therefore, it is important to examine the capacity of nano- and micro-CoCrMo in causing oxidative stress in our cell models. In this case, we used a two-fold approach to assess the induction of oxidative stress using DCF, which serves as a 'generalized' marker for reactive oxygen species,<sup>55</sup> and DHE, which serves as a specific marker of superoxide anions.<sup>56</sup> It seems that the oxidative responses against

nano- and micro-CoCrMo were cell specific: both nano- and micro-CoCrMo resulted in significantly higher DCF levels and DHE levels in OB and M0 cells; significantly higher DCF and DHE levels were observed in macrophages at all concentrations studied (0.1–1000  $\mu\text{g mL}^{-1}$ ). It seems that the OB cells behaved like the M0 immune cells, which are known to exhibit a “respiratory burst” upon phagocytosis of microbes, marked by significant increases in the production of hydrogen peroxide and superoxide anions *via* enzymatic pathways that are critical for initiating anti-microbial response and infection clearance.<sup>57</sup> Meanwhile, corrosion of metal in an aqueous environment could contribute to oxidative stress. Low levels (*e.g.* 0.02  $\mu\text{g mL}^{-1}$ ) of Mo, Co, and Cr ions have been detected in CoCrMo particle solutions after short exposure times (*e.g.* 24 h),<sup>58</sup> and substantial evidence has indicated that metals and metal ions, including Co and Cr, cause oxidative stress *in situ* regardless of the means of exposure.<sup>5,7</sup> In this study, the oxidative stress was likely attributed to the combined effects of nanoparticle exposure and the ions released.

The significantly increased oxidative stress of osteoblasts (OBs) and macrophage (M0) cells may help in explaining the increased risks of implant loosening and osteolysis in orthopaedic implant patients,<sup>4–7</sup> as there is evidence suggesting that the presence of wear particles in the joint fluid stimulates a localized inflammatory response.<sup>4</sup> Localized inflammation promotes osteoclast activity, bone resorption and loosening of the implant.<sup>59</sup> By contrast, BEAS-2B cells had no significant DHE changes but had significantly increased DCF levels at relatively high particle concentrations (*e.g.* 100 and 1000  $\mu\text{g mL}^{-1}$ ). Moreover, nano-CoCrMo caused significantly higher levels of oxidative stress in lung epithelial cells compared to micro-CoCrMo at concentrations of 100 and 1000  $\mu\text{g mL}^{-1}$ , which was consistent with the expected size-dependent effect due to the increased reactive surface area of nano-CoCrMo compared to micro-CoCrMo. No significant differences were found in the DHE assay, which suggests that CoCrMo particles cause oxidative stress *via* species other than superoxide anions. Additionally, we found that these results were consistent with the fibroblast studies in the literature,<sup>51,60</sup> which showed high levels of oxidative stress, marked by increased levels of DCF fluorescence, after as little as 2 h of exposure<sup>60</sup> and increased levels of 8-OHdG staining, a marker of oxidative stress induced DNA damage, after 24 h of exposure to CoCrMo particles.<sup>51</sup> Increased levels of oxidative stress in lung epithelial cells could ultimately lead to downstream effects such as DNA damage and genotoxicity upon long term exposure<sup>11,51,61</sup> and may therefore be a contributing factor in the development of lung disease from pulmonary CoCrMo particle exposure in occupational settings.

## 5. Conclusions

This study examined the toxicity of nano- and micro-CoCrMo and determined whether their exposure induced oxidative stress in human lung epithelial cells, osteoblasts and macrophages. These *in vitro* findings suggest that both nano- and

micro-CoCrMo can induce toxicity and the responses of cell viability and oxidative stress are specific to dose, exposure time and cell type. In future studies, the mechanism of cellular uptake and the cellular distribution and excretion of CoCrMo particles will be investigated. The toxicity of these particles will be further examined in animal models which generally provides a better approximation of what may occur during a real-life exposure situation. For instance, CoCrMo nanoparticles may be injected in a bone implant rat model<sup>62–64</sup> or exposed to the lung in an intra-tracheal instillation rat model<sup>65</sup> to examine their local and systemic toxicity.

## List of abbreviated terms

ATCC	American type tissue collection
CoCrMo	Cobalt chromium molybdenum
DCF	2',7'-Dichlorofluorescein diacetate
DHE	Dihydroethidium
DLS	Dynamic light scattering
DMEM	Dulbecco's modified Eagle's medium
DTP	Dental technician's pneumoconiosis
EDTA	Ethylenediaminetetraacetic acid
FBS	Fetal bovine serum
HMLD	Hard metal lung disease
micro-CoCrMo	CoCrMo microparticles
nano-CoCrMo	CoCrMo nanoparticles
OB	Osteoblast
PBS	Phosphate buffered saline
PMA	Phorbol-12-myristate-13-acetate
SEM	Scanning electron microscopy
TEM	Transmission electron microscopy
WC-Co	Tungsten carbide cobalt

## Competing financial interest

The authors declare no competing financial interest.

## Acknowledgements

We acknowledge financial support from the Department of Defense office of the Congressionally Directed Medical Research Programs (CDMRP), the AO Foundation (Project S-13-15 L was supported by the AO Foundation), the Osteosynthesis & Trauma Care Foundation, the West Virginia National Aeronautics and Space Administration Experimental Program to Stimulate Competitive Research (WV NASA EPSCoR), and CAPES (BEX-5515/10-6). AA thanks the American Foundation for Pharmaceutical Education for her Pre-Doctoral Fellowship in Pharmaceutical Sciences award 2012–2014. We acknowledge the use of the WVU Shared Research Facilities. The authors thank Suzanne Danley for proofreading.

## References

- 1 E. Ingham and J. Fisher, *Proc. Inst. Mech. Eng., Part H*, 2000, **214**, 21–37.

- 2 R. Pourzal, I. Catelas, R. Theissmann, C. Kaddick and A. Fischer, *Wear*, 2011, **271**, 1658–1666.
- 3 G. M. Keegan, I. D. Learmonth and C. P. Case, *Crit. Rev. Toxicol.*, 2008, **38**, 645–674.
- 4 D. Granchi, E. Verri, G. Ciapetti, S. Stea, L. Savarino, A. Sudanese, M. Mieti, R. Rotini, D. Dallari, G. Zinghi and L. Montanaro, *J. Bone Jt. Surg., Br. Vol.*, 1998, **80**, 912–917.
- 5 I. Milosev, R. Trebse, S. Kovac, A. Cor and V. Pisot, *J. Bone Jt. Surg., Am. Vol.*, 2006, **88**, 1173–1182.
- 6 M. Sundfeldt, L. V. Carlsson, C. B. Johansson, P. Thomsen and C. Gretzer, *Acta Orthop.*, 2006, **77**, 177–197.
- 7 H. G. Willert, G. H. Buchhorn, A. Fayyazi, R. Flury, M. Windler, G. Koster and C. H. Lohmann, *J. Bone Jt. Surg., Am. Vol.*, 2005, **87**, 28–36.
- 8 G. Bhabra, A. Sood, B. Fisher, L. Cartwright, M. Saunders, W. H. Evans, A. Surprenant, G. Lopez-Castejon, S. Mann, S. A. Davis, L. A. Hails, E. Ingham, P. Verkade, J. Lane, K. Heesom, R. Newson and C. P. Case, *Nat. Nanotechnol.*, 2009, **4**, 876–883.
- 9 W. V. Christian, L. D. Oliver, D. J. Paustenbach, M. L. Kreider and B. L. Finley, *J. Appl. Toxicol.*, 2014, **34**, 939–967.
- 10 A. E. Goode, J. M. Perkins, A. Sandison, C. Karunakaran, H. K. Cheng, D. Wall, J. A. Skinner, A. J. Hart, A. E. Porter, D. W. McComb and M. P. Ryan, *Chem. Commun.*, 2012, **48**, 8335–8337.
- 11 I. Papageorgiou, V. Shadrack, S. Davis, L. Hails, R. Schins, R. Newson, J. Fisher, E. Ingham and C. Case, *Mutat. Res., Fundam. Mol. Mech. Mutagen.*, 2008, **643**, 11–19.
- 12 A. Sood, S. Salih, D. Roh, L. Lacharme-Lora, M. Parry, B. Hardiman, R. Keehan, R. Grummer, E. Winterhager, P. J. Gokhale, P. W. Andrews, C. Abbott, K. Forbes, M. Westwood, J. D. Aplin, E. Ingham, I. Papageorgiou, M. Berry, J. Liu, A. D. Dick, R. J. Garland, N. Williams, R. Singh, A. K. Simon, M. Lewis, J. Ham, L. Roger, D. M. Baird, L. A. Crompton, M. A. Caldwell, H. Swalwell, M. Birch-Machin, G. Lopez-Castejon, A. Randall, H. Lin, M. S. Suleiman, W. H. Evans, R. Newson and C. P. Case, *Nat. Nanotechnol.*, 2011, **6**, 824–833.
- 13 C. Brown, L. Lacharme-Lora, B. Mukonoweshuro, A. Sood, R. B. Newson, J. Fisher, C. P. Case and E. Ingham, *Biomaterials*, 2013, **34**, 8564–8580.
- 14 A. H. Hosman, S. K. Bulstra, J. Sjollema, H. C. van der Mei, H. J. Busscher and D. Neut, *J. Orthop. Res.*, 2012, **30**, 341–347.
- 15 B. Scharf, C. C. Clement, V. Zolla, G. Perino, B. Yan, S. G. Elci, E. Purdue, S. Goldring, F. Macaluso, N. Cobelli, R. W. Vachet and L. Santambrogio, *Sci. Rep.*, 2014, **4**, 5729.
- 16 K. Morgenroth, H. Kronenberger, G. Michalke and R. Schnabel, *Pathol., Res. Pract.*, 1985, **179**, 528–536.
- 17 A. Selden, W. Sahle, L. Johansson, S. Sorenson and B. Persson, *Chest*, 1996, **109**, 837–842.
- 18 M. R. Cullen, *Chest*, 1984, **86**, 513–514.
- 19 P. Galy, J. Bourret, F. Tolot, J. Brune, R. Girard, H. Rousset, T. Wiesendanger and G. Dorsit, *Rev. Inst. Hyg. Mines*, 1974, **29**, 130–137.
- 20 A. I. Selden, B. Persson, S. I. Bornberger-Dankvardt, L. E. Winstrom and L. S. Bodin, *Thorax*, 1995, **50**, 769–772.
- 21 L. Geraets, A. G. Oomen, J. D. Schroeter, V. A. Coleman and F. R. Cassee, *Toxicol. Sci.*, 2012, **127**, 463–473.
- 22 T. L. Knuckles, J. H. Yi, D. G. Frazer, H. D. Leonard, B. T. Chen, V. Castranova and T. R. Nurkiewicz, *Nanotoxicology*, 2012, **6**, 724–735.
- 23 P. A. Stapleton, V. C. Minarchick, M. Mccawley, T. L. Knuckles and T. R. Nurkiewicz, *Microcirculation*, 2012, **19**, 126–142.
- 24 A. L. Armstead, C. B. Arena and B. Y. Li, *Toxicol. Appl. Pharmacol.*, 2014, **278**, 1–8.
- 25 T. Hamza and B. Li, *BMC Microbiol.*, 2014, **14**, 207.
- 26 T. Hamza, M. Dietz, D. Pham, N. Clovis, S. Danley and B. Li, *Eur. Cells Mater.*, 2013, **25**, 341–350; discussion 350.
- 27 J. Noore, A. Noore and B. Li, *Antimicrob. Agents Chemother.*, 2013, **57**, 1283–1290.
- 28 H. S. Li, H. Ogle, B. B. Jiang, M. Hagar and B. Y. Li, *J. Orthop. Res.*, 2010, **28**, 992–999.
- 29 F. Likibi, B. B. Jiang and B. Y. Li, *J. Mater. Res.*, 2008, **23**, 3222–3228.
- 30 N. Hondow, R. Brydson, P. Y. Wang, M. D. Holton, M. R. Brown, P. Rees, H. D. Summers and A. Brown, *J. Nanopart. Res.*, 2012, **14**, 977.
- 31 T. A. Simoes, A. P. Brown, S. J. Milne and R. M. D. Brydson, *J. Phys.: Conf. Ser.*, 2015, **644**, 012039.
- 32 A. Albanese, P. S. Tang and W. C. W. Chan, *Annu. Rev. Biomed. Eng.*, 2012, **14**, 1–16.
- 33 V. Castranova, *J. Occup. Environ. Med.*, 2011, **53**, S14–S17.
- 34 A. G. Cattaneo, R. Gornati, E. Sabbioni, M. Chiriva-Internati, E. Cobos, M. R. Jenkins and G. Bernardini, *J. Appl. Toxicol.*, 2010, **30**, 730–744.
- 35 G. Oberdorster, *Regul. Toxicol. Pharmacol.*, 1995, **21**, 123–135.
- 36 A. M. Gatti and F. Rivasi, *Biomaterials*, 2002, **23**, 2381–2387.
- 37 D. Choudat, *Tuber. Lung Dis.*, 1994, **75**, 99–104.
- 38 D. M. Mosser, *J. Leukocyte Biol.*, 2003, **73**, 209–212.
- 39 C. Hinuber, C. Kleemann, R. J. Friederichs, L. Haubold, H. J. Scheibe, T. Schuelke, C. Boehlert and M. J. Baumann, *J. Biomed. Mater. Res., Part A*, 2010, **95**, 388–400.
- 40 M. J. Allen, B. J. Myer, P. J. Millett and N. Rushton, *J. Bone Jt. Surg., Br. Vol.*, 1997, **79**, 475–482.
- 41 W. N. Rom, J. E. Lockey, J. S. Lee, A. C. Kimball, K. M. Bang, H. Leaman, R. E. Johns, Jr., D. Perrota and H. L. Gibbons, *Am. J. Public Health*, 1984, **74**, 1252–1257.
- 42 D. Sherson, N. Maltbaek and K. Heydorn, *Eur. Respir. J.*, 1990, **3**, 1227–1229.
- 43 C. Buzea, I. I. Pacheco and K. Robbie, *Biointerphases*, 2007, **2**, MR17–MR71.
- 44 G. Oberdorster, J. Ferin and B. E. Lehnert, *Environ. Health Perspect.*, 1994, **102**, 173–179.
- 45 G. Oberdorster, E. Oberdorster and J. Oberdorster, *Environ. Health Perspect.*, 2005, **113**, 823–839.
- 46 A. J. Wagner, C. A. Bleckmann, R. C. Murdock, A. M. Schrand, J. J. Schlager and S. M. Hussain, *J. Phys. Chem. B*, 2007, **111**, 7353–7359.
- 47 M. Geiser, *Microsc. Res. Tech.*, 2002, **57**, 512–522.
- 48 I. Canton and G. Battaglia, *Chem. Soc. Rev.*, 2012, **41**, 2718–2739.

- 49 C. Cervellati, G. Bonaccorsi, E. Cremonini, A. Romani, E. Fila, M. C. Castaldini, S. Ferrazzini, M. Giganti and L. Massari, *BioMed Res. Int.*, 2014, 569563, DOI: 10.1155/2014/569563.
- 50 A. Tsaousi, E. Jones and C. P. Case, *Mutat. Res., Genet. Toxicol. Environ. Mutagen.*, 2010, **697**, 1–9.
- 51 I. Papageorgiou, C. Brown, R. Schins, S. Singh, R. Newson, S. Davis, J. Fisher, E. Ingham and C. P. Case, *Biomaterials*, 2007, **28**, 2946–2958.
- 52 M. A. Germain, A. Hatton, S. Williams, J. B. Matthews, M. H. Stone, J. Fisher and E. Ingham, *Biomaterials*, 2003, **24**, 469–479.
- 53 J. S. Brody and A. Spira, *Proc. Am. Thorac. Soc.*, 2006, **3**, 535–537.
- 54 D. Lison, *Crit. Rev. Toxicol.*, 1996, **26**, 585–616.
- 55 X. P. Chen, Z. F. Zhong, Z. T. Xu, L. D. Chen and Y. T. Wang, *Free Radical Res.*, 2010, **44**, 587–604.
- 56 X. Q. Chen, X. Z. Tian, I. Shin and J. Yoon, *Chem. Soc. Rev.*, 2011, **40**, 4783–4804.
- 57 K. E. Iles and H. J. Forman, *Immunol. Res.*, 2002, **26**, 95–105.
- 58 T. A. Simoes, M. G. Bryant, A. P. Brown, S. J. Milne, M. Ryan, A. Neville and R. Brydson, *Acta Biomater.*, 2016, **45**, 410–418.
- 59 D. Cadosch, E. Chan, O. P. Gautschi and L. Filgueira, *J. Biomed. Mater. Res., Part A*, 2009, **91**, 1252–1262.
- 60 V. K. Raghunathan, M. Devey, S. Hawkins, L. Hails, S. A. Davis, S. Mann, I. T. Chang, E. Ingham, A. Malhas, D. J. Vaux, J. D. Lane and C. P. Case, *Biomaterials*, 2013, **34**, 3559–3570.
- 61 M. Figgitt, R. Newson, I. J. Leslie, J. Fisher, E. Ingham and C. P. Case, *Mutat. Res.*, 2010, **688**, 53–61.
- 62 B. Li, B. Jiang, B. M. Boyce and B. A. Lindsey, *Biomaterials*, 2009, **30**, 2552–2558.
- 63 B. Li, B. Jiang, M. J. Dietz, E. S. Smith, N. B. Clovis and K. M. Rao, *J. Orthop. Res.*, 2010, **28**, 48–54.
- 64 B. M. Boyce, B. A. Lindsey, N. B. Clovis, E. S. Smith, G. R. Hobbs, D. F. Hubbard, S. E. Emery, J. B. Barnett and B. Li, *J. Orthop. Res.*, 2012, **30**, 196–202.
- 65 A. L. Armstead, V. C. Minarchick, D. W. Porter, T. R. Nurkiewicz and B. Li, *PLoS One*, 2015, **10**, e0118778.